RSC Advances

ROYAL SOCIETY OF CHEMISTRY

www.rsc.org/advances

Self Organization of Main-chain/Side-chain Liquid Crystalline Polymer Based on "Jacketing" Effect with Different Lengths of Spacer: From Smectic to Hierarchically Ordered Structure

He-lou Xie[a*], Bin Ni[a], Quan Liu[a], Jun Wang [b], Shuang Yang[b], Hai-liang Zhang[a*], Er-qiang Chen[b*]

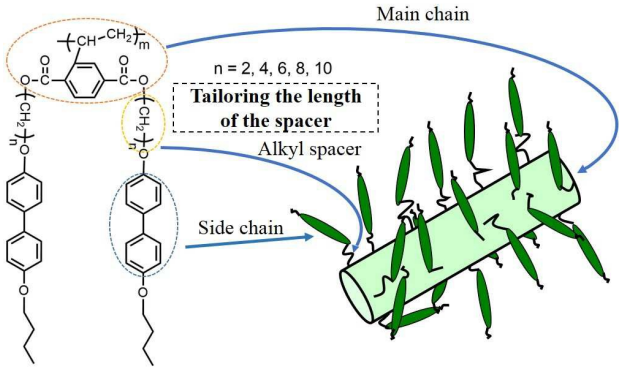

Journal Name

ARTICLE

Self Organization of Main-chain/Side-chain Liquid Crystalline Polymer Based on "Jacketing" Effect with Different Lengths of Spacer: From Smectic to Hierarchically Ordered Structure

He-lou Xie[a*], Bin Ni[a], Quan Liu[a], Jun Wang[b], Shuang Yang[b], Hai-liang Zhang[a*], Er-qiang Chen[b*]

Received 00th January 20xx,
Accepted 00th January 20xx

DOI: 10.1039/x0xx00000x

www.rsc.org/

Abstract: A series of combined main-chain/side-chain liquid crystalline polymers (MCSCLCP) based on side-chain "Jacketing" effect, poly{(2,5-bis[n-(4-butoxy-4' -oxybiphenyl)n-alkyl]oxycarbonyl}styrene) with different lengths of alkyl spacers (denoted as P*n*, *n* represents the number of carbon atoms in the alkyl spacers, *n* = 2 ~ 10) have been successfully synthesized via atom transfer radical polymerization (ATRP). The chemical structures of P*n*s and the corresponding monomers were characterized using combined techniques with satisfactory analysis data. The phase structures and transitions of P*n* were investigated using differential scanning calorimetry (DSC), polarized optical microscope (POM), and one- and two-dimensional wide-angle X-ray diffraction (1D and 2D WAXD). It has been identified that P2 and P4 with short alkyl spacers form typical smectic phase. For *n* ≥ 6, P*n*s exhibit similar hierarchical ordered structure at low temperatures, bearing double orderings on the nanometer and sub-nanometer scales. In the hierarchical structure, the main-chains based on "jacketing" effect form a 2D centered rectangular scaffold, and the side-chain biphenyl mesogens within the scaffold pack into a smectic E-like structure. The *a* dimension of rectangular lattice enlarges with *n*. When the temperature is increased, different from P6, P8 and P10 present the same phase behavior, forming smectic B-like packing of side chains and maintaining their main-chain scaffold until isotropization.

Key word: combined main-chain/side-chain liquid crystalline polymers, "Jacketing" Effect, Different Lengths of Spacer

Introduction

Liquid crystalline polymers (LCPs) as functional materials combining the liquid crystalline (LC) behavior and polymeric property have obtained extensive application as engineering plastics, high-modulus and high-strength fibers, nonlinear optic or electro-optic materials, stationary phases, gas separation membranes, etc.[1, 2] The performance of LCPs is dependent on their anisotropic properties

[a]*Key Laboratory of Special Functional Polymer Materials of Hunan Province, Key Laboratory of Advanced Functional Polymer Materials of Colleges and Universities of Hunan Province and Key Lab of Environment-friendly Chemistry and Application in Ministry of Education, College of Chemistry, Xiangtan University, Xiangtan 411105, Hunan Province, China.*
** To whom the correspondence should be addressed.*
E-mail: xhl20040731@163.com (HLX)
DOI: 10.1039/x0xx00000x

and self-assembling supramolecular structure. Thus, how to rationally design and adjust the self-assembling supramolecular structure of LCPs becomes an important subject in both practical application and fundamental research.[3-10] In order to control the supramolecular structures, different architectural LCPs have been designed and synthesized. The classical types of LCPs are main-chain LC polymers (MCLCPs) with the mesogens embedded into the backbone of a polymer chain and side-chain LC polymers (SCLCPs) with the mesogens attached to the main chain as side groups.[11-13] For SCLCP, the mesogen can be either longitudinally (end-on) or laterally (side-on) linked to the polymer backbone, respectively.[14-18] It is worth noting that decreasing the length of the spacers between the backbone and side-on side chain can lead to a significant "jacketing" effect given by the side chains on the polymer backbone. Typically, this effect is encountered in mesogen-jacketed LCPs (MJLCPs).[19-25] As for MJLCPs, the rodlike mesogenic groups are laterally attached to the flexible backbone via a short linkage or a single carbon-carbon bond, which can force the polymer chain to stretch along the main-chain direction. Thus, the backbone and side groups of MJLCP almost fuse together to become a single conformational unit which is cylinder-like. Consequently, MJLCPs can readily form columnar phases rather than conventional smectic or nematic phases observed in SCLCPs.

Combined main-chain/side-chain LC polymer (MCSCLCP)[26-34] is a hybrid one combining the chemical features of MCLCP and SCLCP. MCSCLCP is usually prepared by condensation polymerization method. From the chemical viewpoint, the main chain of MCSCLCP can either be rigid rod or possess an alternative structure of rod-like mesogenic groups with flexible spacers; and its side chain is usually composed of mesogenic group linked to the main-chain repeating unit through a flexible spacer. Compared with MCLCP and SCLCP, the interplay between main- and side-chain of MCSCLCP becomes more complicated, which leads to versatility of the LC properties and supramolecular structures. Recently, we have proposed that MCSCLCP can be synthesized based on chain polymerization.[35-37] The first example is poly(2,5-bis{[6-(4-butoxy-4'- oxybiphenyl) hexyl]oxycarbonyl}styrene) (PBBHCS). Experimental results reveal that PBBHCS with sufficiently high molecular weight (MW) can self-assemble into a hierarchical structure containing double orderings on the nanometer and sub-nanometer scales.[36] Taking the advantage of "jacketing" effect, the rodlike main chain of PBBHCS is generated by the central rigid portion of the side chains laterally attached to every second carbon atom along the polyethylene backbone. At low temperatures, the main chains can form a two-dimensional (2D) scaffold with centered rectangular arrangement on the nanometer scale, and the biphenyl-containing side chains fill in the space between the main chains, forming a smectic E (SmE)-like structure with the side-chain axis perpendicular to that of main chain. It is further found that incorporating different functional components into the side chain, such as azobenzene mesogen, triphenylene (Tp) mesogen and polyhedral oligomeric silsesquioxane (POSS) can also offer interesting property.[37-39]

It is well known that the length of flexible spacer of LCP plays an important role in determining the LC behaviours of LCP.[40-46,] The decoupling effect proposed by Finkelmann et al. Elucidates that the flexible spacer with sufficiently long length can efficiently decrease the dynamics interaction between main chain and mesogenic side groups, beneficial to the LC formation in SCLCPs.[47, 48] It should be worth noting that for the MCSCLCP with the main chain based on "jacketing" effect, the "flexible spacer" takes part in two roles. On one hand, the flexible spacer can facilitate the LC phase formation of mesogenic side chains. On the other hand, it may also affect the packing of main chains. In order to further excavate the effect of spacer, we synthesized a series of MCSCLCP bearing the spacers with different lengths, poly(2,5-bis{[n-(4-butoxy-4'-oxybiphenyl)n-alkyl] oxycarbonyl}styrene (denoted as P*n*, *n* represents the number of carbon atoms in the alkyl spacers, *n* = 2 ~ 10), of which the chemical structure is shown in Scheme 1. The phase structures and transitions of P6 (i.e., PBBHCS mentioned above) has been well studied.[36] Here, using P6 as the reference, we attempt to elucidate how the variation of spacer length will influence the molecular packing behavior. We find that with short spacers P2 and P4 just form smectic structure. For P8 and P10, the hierarchical structure containing double orderings on the nanometer and sub-nanometer scales, which is similar to that of P6, is demonstrated at low temperatures. Moreover, different from P6, P8 and P10 allows the biphenyl mesogen packing in a smectic B (SmB)-like structure after the melt of their SmE-like structure, and the main-chain scaffolds remain until isotropic temperature.

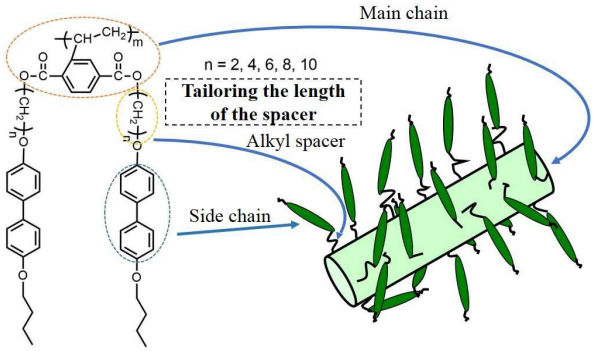

Scheme 1. The chemical structure and schematic draw of P*n* (*n* = 2, 4, 6, 8, 10).

Experimental

Materials

4,4'-Biphenol (98%, Alfa Aesar), Bromobutane (98%, Alfa Aesar), 1,2-Dibromoethane (98%, Alfa Aesar), 1,4-Dibromobutane (98%, Alfa Aesar), 1,6-Dibromohexane (98%, Alfa Aesar), 1,8-Dibromooctane (98%, Alfa Aesar), 1,10-Dibromodecane (98%, Alfa Aesar), 1-Bromoethylbenzene (BEB, 98%, Acros) were used as received. Sparteine (Spt, 98%, Aldrich) was distilled under reduced pressure over calcium hydride and stored under a nitrogen atmosphere at 4 °C in the dark. CuBr was prepared from CuBr2 and

purified by stirring in acetic acid, washing with methanol, and then dried in vacuo. N,N-dimethylformamide (DMF) (Shanghai Chemical Reagents Co., A.R. grade) were used without further purification. Acetone (AR; Beijing Chemical Co.) was refluxed over potassium permanganate and distilled before used. Chlorobenzene (Acros, 99%) was purified by washing with concentrated sulfuric acid to remove residual thiophenes, followed by washing twice with water, once with 5% sodium carbonate solution, and again with water before being dried with anhydrous calcium chloride and then distilled.

Instruments and Measurements

^{1}H NMR (400 MHz) and ^{13}C NMR (100 MHz) experiments were carried out on a BRUKER ARX spectrometer at room temperature using chloroform-d ($CDCl_3$) as the solvent and tetramethylsilane (TMS) as the internal standard. Elemental analysis was carried out with an Elementar Vario EL instrument. The apparent number-average MW (M*n*) and MW distribution were measured by GPC (WATERS 1515) instrument calibrated by polystyrene standards. THF was used as the eluent and the elution speed was 1.0 ml/min at 38 °C.

LC texture of the polymers were recorded under polarized optical microscopy (POM, Leica DM-LM-P) coupled with a Mettler-Toledo hot stage (FP82HT). For POM experiments, the film samples with the thickness of ~10 μm were obtained via cast-coating followed by slow drying at room temperature. The thermal transitions of the polymers were detected by differential scanning calorimetry (DSC, TA-Q10). Samples were encapsulated in sealed aluminum pans with a typical mass of 3-10 mg. The temperature and heat flow were calibrated using standard materials (indium and zinc) at cooling and heating rates 10 °C/min.

One-dimensional (1D) wide-angle X-ray diffraction (WAXD) experiments were carried out on a Bruker D8 advance diffraction with a 3 kW ceramic tube as the X-ray source (Cu Kα) and lynxeye detector as the detector. The reflection peak positions were calibrated with silicon powder (2θ > 15°) and silver behenate (2θ < 10°). Background scattering was subtracted from the sample patterns. A temperature control unit (Paar Physica TCU 100) connected with the diffractometer was exploited to study the structure evolutions as a function of temperature. 2D-WAXD shear patterns were obtained using a Bruker D8Discover diffraction with a Vantec-500 detector. The positions of diffraction patterns were calibrated using the same method mentioned above. The samples were put on the sample stage, and the point-focused X-ray beam was aligned perpendicular or parallel to the mechanical shearing or fiber direction. The 2D diffraction patterns were recorded in a transmission mode at different temperatures upon heating and cooling.

Experimental section

Synthesis

The synthetic route of the monomers (M*n*, *n* = 2, 4, 6, 8, 10) and polymers (P*n*s) is outlined in Scheme 2. The detailed information about the monomers is shown in Supporting Information. P*n*s were synthesized via atom transfer radical polymerization reaction (ATRP) with α-bromoethylbenzene as for the initiator and a CuBr/spartein as the catalyst. Here, we used P2 as an example to show the process of the polymerization experiment. M2, CuBr, ethyl bromidebenzene, Spartein were added to a dry tube which was accorded to the ratio of 1: x: 1: 2 (x was the theoretical degree of polymerization of P2), and the chlorobenzene as the solution. Subjected to three cycles of freeze-vacuum-nitrogen before sealing, the polymer tube was placed in the constant temperature of 110 °C. After a certain reaction time, open the sealed tube. The polymer solution was passed through a column of Al_2O_3 to remove the clathrate of CuBr, and then precipitated in the petroleum ether, filtration, washing, vacuum drying. Yield 70%.

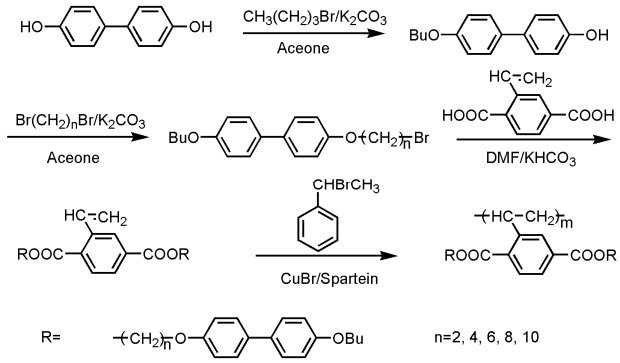

Scheme 2. Synthetic route of the monomers and the polymers.

Results and Discussion

Synthesis of the monomers and Polymers

In our previous work, P6 samples with different MWs have synthesized via ATRP. According to the similar synthetic method, in this article, a series of P*n*s with different lengths of the alkyl spacers have been synthesized in good-to-excellent yields through multistep reaction (see Scheme 1). The detailed synthetic process and chemical characterization are shown in Supporting Information. The chemical structure, MW and polydispersity of the resultant polymers were characterized by ^{1}H NMR and GPC. Herein, using P2 and its corresponding monomer M2 as the example, the ^{1}H NMR spectra are shown in Figure 1. For the monomer, the peaks at 8.24 ppm (peak i), 7.92 ppm (peak h), 7.45 ppm (peak e), 6.94 ppm (peak f) are the characteristic peaks of the benzene ring hydrogen displacement, while those at 6.67 ppm (peak m), 5.75 ppm (peak k), 5.42 ppm (peak j) belong to vinyl substituent. All peaks area ratio with the number of hydrogen atoms match very well with the chemical structure of M2. After polymerization, the distinct change is the disappearance of the peaks of the vinyl substituent and meanwhile, other peaks become quite broad. This indicates that the

polymer is synthesized successfully. The other monomers and polymers with different alkyl spacers present similar NMR results (see Supporting Information). The GPC traces showed that all the P*n*s were unimodal with relatively narrow MW distribution, indicating a good agreement with the rule of ATRP.[49] The GPC measured MW and polydispersity indexs of P*n*s are summarized in Table 1. The thermal stability of P*n*s was investigated with TGA. For all the samples, the temperatures at 5% weight loss were higher than 370 and 300 °C in nitrogen and in air atmosphere, respectively (see Table 1).

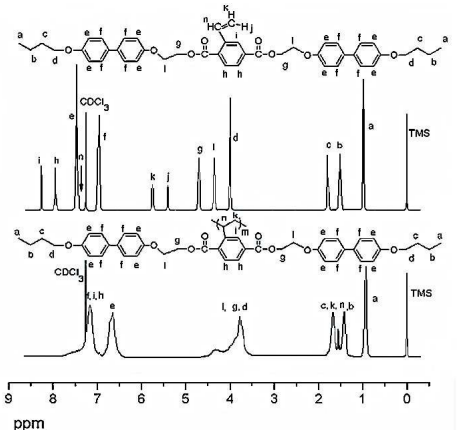

Figure 1. ^{1}H NMR spectra of P2 and the corresponding monomer M2.

Table1. GPC Results and Thermotropic Property of Pn (n =2, 4, 6, 8, 10).

Sample	Yield[a] (%)	$M_{n,GPC}$[b] ($\times10^4$)	M_w/M_n[b]	Phase Transition (°C)	$T_{d,N2}$[d] (°C)	$T_{d,air}$[e] (°C)
P2	70	1.90	1.10	SmA(192 °C)isotropic	371	308
P4	65	1.51	1.15	SmA(187 °C) isotropic	362	301
P6	65	1.55	1.06	LC1[f](136 °C)LC2[g](161 °C) SmA(172 °C)isotropic	377	294
P8	68	2.02	1.13	LC1[f](130 °C)LC3[h](136 °C) LC2[g](171 °C) isotropic	381	303
P10	65	2.21	1.15	LC1[f](116 °C)LC3[h](132 °C) LC2[g](186 °C) isotropic	387	299

[a] Yield calculated according to previous paper;[39] [b] Obtained from GPC with linear PS as standards; [c] Phase transitions and corresponding transition temperature evaluated by DSC at a rate of 10 °C/min under heating; [d,e] The temperature at which 5% weight loss of the sample was reached from TGA under nitrogen atmosphere and air atmosphere, respectively. [f] Orthogonal SmE-like structure of side-chain mesogens fills in 2D centered rectangular scaffold of main chain; [g] Smectic side-chain mesogens fills in 2D centered rectangular scaffold of main chain; [h] Hexagonal SmB-like structure of side-chain mesogens fills in 2D centered rectangular scaffold of main chain.

Overall Phase Transition Behavior of Pn

DSC experiment was used to examine the phase transitions of P*n*s. The results show that all the first-order transitions are enantiotropic. P6 has been carefully analyzed in our previous work. Herein, P6 is used as the reference. Comparison between P6 and other P*n*s will help to elucidate the length effect of flexible spacers. The previous results of P6 reveal that three first-order transitions during heating can be ascribed as follows: highly ordered LC phase combining the 2D centered rectangular main-chain scaffold with SmE-like packing of the side chains → 2D centered rectangular scaffold of main chain → SmA → isotropic state. The DSC cooling and subsequent heating traces of P2, P4, P8, and P10 at a cooling/heating rate of 10 °C/min are shown in Figure 2 and Figure S1. It is noted that P8 and P10 with relative longer spacer exhibits apparently the phase transition similar to P6 (the detailed difference between them will be discussed below). For example, three first-order transitions of P10 are observed during the heating and cooling process, with the transition temperatures are obviously different from those of P6 (Figure 2b). On the other hand, P2 and P4 with short spacer present only one LC transition. For P2 (Figure 2a), a glass transitions at 160 °C and one first-order transition at 192 °C can be observed during the heating process. The DSC curves of P4 and P8 are shown in Supporting Information. The phase transition temperatures of Pns are listed in Table 1.

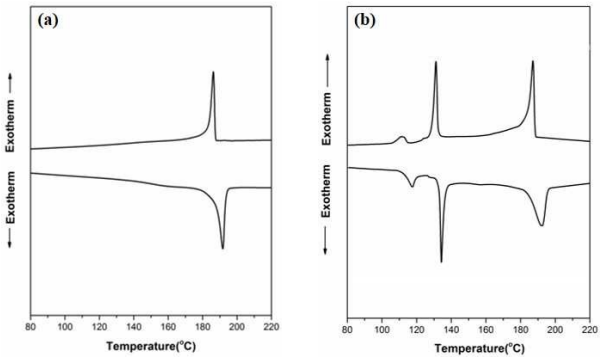

Figure 2. DSC thermograms of P2 (a) and P10 (b) at a rate 10 °C/min during cooling and subsequent heating process.

POM results also implied the phase variation tendency of P*n*s similar to that revealed by DSC. Below the highest transition temperature, all the samples presented strong birefringence under POM, indicating the existence of LC phases. At different temperatures, the five P*n*s may exhibit different textures. The distinct change of textural color of P6 has been observed when the sample went through different temperature areas.[36] P8 and P10 displayed the typical the fan-shaped texture at room temperature. Upon heating, the texture became significantly different when the samples crossed over the low- and middle-temperature transitions. The representative POM images of P10 at different temperatures are shown in Figure 3a-c. However, P2 and P4 showed grainy textures until up to the isotropic temperature, and the texture did not change during the heating or cooling process. Figure 3d is a POM image of P2 at room temperature. The POM results are good consistent with the DSC results.

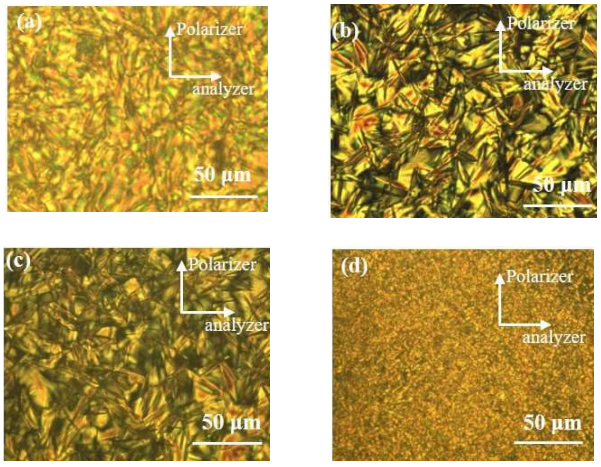

Figure 3. Representative textures of P10 at 30 °C (a), 130 °C (b), 170 °C (c) and P2 at 170 °C (d), (200 × magnification).

1D WAXD thermal experiment was performed to elucidate the phase behavior. Similar to P6,[36] P8 and P10 presented two sets of diffractions in both the low- and high-angle areas, respectively. The 1D WAXD profiles of P10 recorded at various temperatures are shown in Figure 4a. At low temperatures, four distinct diffraction peaks have been observed in the low-angle region, of which the q-ratio (q = 4πsinθ/λ) is 1:1.38:1.92:2 at room temperature, indicating a LC phase structure other than lamellar and hexagonal. On the other hand, the diffractions in the high-angle region at low temperatures are highly reminiscent of that of biphenyl containing SCLCPs forming a SmE phase.[50-52] From left to right, the three peaks can be assigned as (11), (20), and (21) diffractions of SmE. When the temperature is located between 30 and 110 °C, there are hardly change of the diffraction peaks for both low- and high-angle region. From 120 to 130 °C, the low-angle diffractions slightly shift to left due to thermal expansion. Meanwhile, the two peaks at 2θ of 20.81° and 26.66° disappear, only the diffraction peak of 19.58° is still kept. This outcome suggests that the SmE ordered structure of the side chain transforms into another one, which can be smectic B (SmB).[53, 54] With further increasing temperature, the first low-angle diffraction gradually reduces its intensity, but others peaks always remains. In the meantime, the peak at 19.58° becomes very diffuse, indicating that the SmB structure of biphenyl mesogens is destroyed. When the temperature exceeds 200 °C, only scattering holes appear in the high- and low-angle region, respectively, indicating that the sample enters isotropic state. In Figure 4b, the d-spacing and the full-width of half-height (FWHH) of the first peak in the high-angle region is plotted as functions of temperature. Three dramatic jumps of the d-spacing and FWHH have been observed, indicating the three transitions which well agree with the results observed in DSC (see the dashed vertical lines). Similar experimental results of P8 are shown in Figure S4.

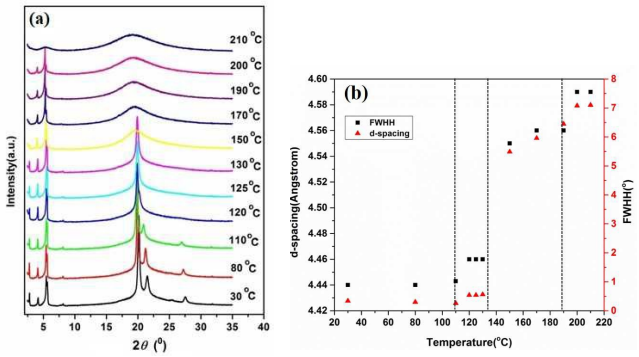

Figure 4. (a) Set of 1D WAXD powder patterns of P10 at different temperatures recorded upon heating; (b) d-spacing and full width of half-height (FWHH) of the first high-angle diffraction as functions of temperature.

For P2 and P4 with short spacer, they presented different diffractive behaviour from P6, P8 and P10. As show in Figure 5, P2 exhibits three peaks in the low angle region with the q-ratio of 1: 2: 3, indicating that P2 forms a lamellar structure (smectic phase). In the high angle region, a scattering halo appears implying the smecitc structure is low ordered. With increasing temperature, the high-angle halo becomes broader and continuously shifts to left side. On the other hand, the three peaks with the q-ratio of 1: 2: 3 in the low-angle region remain during heating. They disappear until

the temperature is higher than 180 °C, indicating the transition from smectic to isotropic. The 1D WAXD result of P4 is shown in Figure S3, similar to that shown in Figure 5.

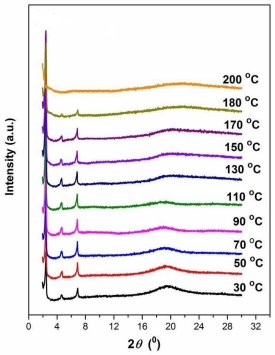

Figure 5. Set of 1D WAXD powder patterns of P2 at different temperatures.

Phase Structure Identification of P*n*

Due to the lack of exact spatial dimension in the 1D WAXD experiment, the detail interpretation about the LC structure could not be obtained. 2D WAXD analysis was performed to further investigate the chain packing of P*n*s. The exact packing structure of P6 has been obtained on basic of 2D WAXD experimental result.36 Here in, we focus on the structure analysis of P2, P4, P8 and P10. To align the LC domains, the samples were mechanically sheared with mild external force at a temperature just below the isotropic temperature. The sheared samples were then annealed at properly selected temperatures for several hours, allowing the LC structures to be fully developed. Figure 6 shows the 2D WAXD patterns of the oriented P10 at different temperatures with the incident X-ray beam perpendicular to the shear direction (along the meridian). At 30 °C, diffraction arcs appear in both the low- and high-angle region as shown in Figure 6a. Using the diffraction of P6 as the reference, the low-angle diffraction arcs can be assigned to (20), (11), (31) and (40) of a rectangular 2D lattice with a = 6.26 nm and b = 2.20 nm, which shall be composed of the main chains.36 Note that the low-angle diffractions are concentrated on the equator. Therefore, the main chains are aligned along the shear direction. The three pairs of diffraction arcs in the high angle region can be assigned as (11), (20), and (21) diffractions of SmE-like structure, respectively. However, at 125 °C only one pair of high-angle diffraction arc located on the meridian can be observed (Figure 6b), suggesting that the side chains form a SmB structure which ae perpendicular to the main chain. After the temperature is increased to 170 °C, the diffraction in the high-angle region becomes very diffuse, while the low-angle diffractions still exist (Figure 6c). This means that the ordered packing of biphenyl mesogens is melted and the ordered scaffold structure formed by main chain is kept. Further heating to above 200 °C will cause all diffractions to disappear. On the basis of the experimental results, the sequence of phase transitions of P10 can be as following: SmE-like structure (side chain) + 2D centered rectangular scaffold (main chain) ↔ SmB-like structure + 2D centered rectangular scaffold ↔ 2D centered rectangular scaffold of main chain ↔ isotropic state. Similar results of P8 can also be observed (see Supporting Information).

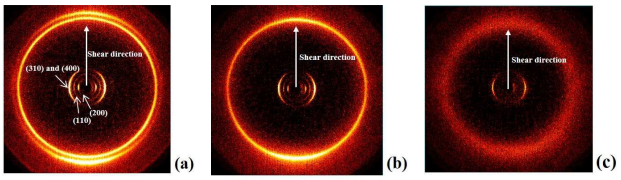

Figure 6. 2D WAXD patterns of P10 recorded with X-ray beam parallel to the X-direction at 30 °C (a); 125 °C (b); 170 °C (c).

The schematic draw of the P8 and P10 chain packing at low temperatures is shown in Figures 7a and 7b. In order to understand more the molecular packing, the relative electron density map of P10 was reconstructed based on the 1D WAXD data, of which the result is shown in Figure 7c (for P8, see Supporting Information). According to chemical structure, the red circular and green area in Figure 7c with the relatively high electron density should be the column constructed by the main chain. It can be calculated that the area (i.e., red + green) is about 1.3 nm^2, in agreement with the main-chain dimension estimated in our previous work.[36] The location nearby the main-chain column (blue area) has the lowest electron density, which could be assigned to the flexible spacer. The blue area has the size of ~ 1 nm, which is close to the length of 1.2 nm for the flexible spacer with all *trans* conformation. The green colored zig-zag areashould correspond to the parallel packing of the biphenyl groups.

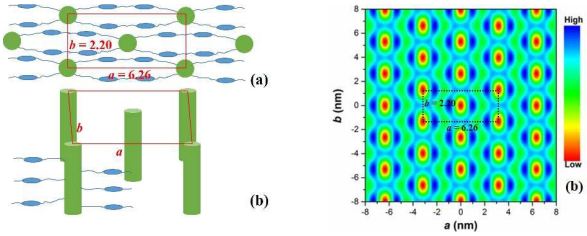

Figure 7. Proposed molecular packing of P8 and P10, (a) top view (the lattice parameters shown therein are for P10); (b) side view. Relative electron density map reconstructed based on the 1D WAXD results of P10 (c).

With the decrease of spacer length, P2 and P4 presented totally different diffraction patterns from P6, P8 and P10. As shown in Figure 8a, three pairs of sharp diffraction arcs of P2 in the low-angle region show on the equator with the q-ratio of 1: 2: 3, confirming the lamellar structure. In addition, a pair of diffuse halo at the high angle appears on the meridian, indicating that the side chains are largely parallel to the normal of smectic layer. Therefore, P2 forms a SmA phase. Assuming the spacer and tail of side chain takes all *trans* conformation, the calculated side-chain length of P2 is 5.37 nm. The experimental measured d-spacing of 3.65 nm is smaller

than the calculated value but larger than a half of it. Thus, P2 should adopt partially interdigitated packing of smectic phase (SmAd). The reconstruction of relative electron density map of P2 is shown in Figure 8b. We assume that the zone with high electron density (red colored) is ascribed to the biphenyl mesogens which are parallel packed to each other. The zone thickness of ~1.4 nm is larger than the size of biphenyl (~1 nm), implying the interdigitated packing. The blue colored area should be occupied by the alkyl spacers, and the area between two adjacent blue zones belongs to the main chains. During the heating process, this diffraction pattern hardly changed until isotropization, meaning P2 forms a stable SmAd phase during the whole area below the isotropic temperature. The 2D WAXD results and reconstructed relative electron density map of P4 are similar to that of P2 (see Supporting Information).

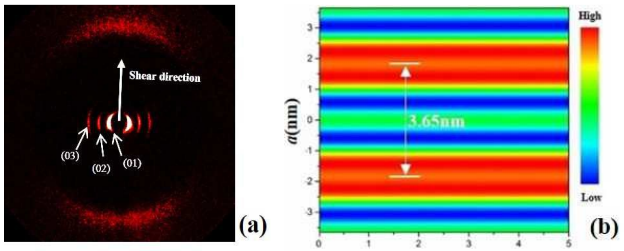

Figure 8. 2D WAXD pattern of P2 recorded with X-ray beam perpendicular to the shear direction at room temperature. (b) Relative electron density map of the smectic phase of P2.

Combined DSC and 1D/2D WAXD results, the phase transition sequences of P*n*s and the LC structure parameters at low temperatures are summarized in Tables 1 and 2, respectively. Obviously, the spacer length plays an important role in the formation of supramolecular structures of this type of MCSCLCP. It has proved that the decoupling effect of spacer length can affect the molecular shape, resulting in the formation of the different supramolecular structure. Herein, the short spacer length with ethylidene or butylidene cannot provide effectively the decoupling effect. The side chains can either extend or fold in the smecitc phase. While the former one can result in the two biphenyl groups towards two opposite directions,[57, 58] the later one makes a hairpin shape of the side chain. In both cases, the side chain packing will be influenced by the polyethylene backbone, and the detailed molecular arrangement of the resultant SmAd is not clear at this moment. For $n \geq 6$, the microphase separation from the side chain and main chain is able to occur and meanwhile, the alkyl spacer may partly involve in the construction of rod-like main chain. Thus, the whole molecular shape of P*n* dramatically changes. The synergistic effect of the main and the side chain facilitates the formation of hierarchically ordered structure. Careful analysis can find the dimension of the ordered structures is dependent on the spacer length. Figure 9a describes the d-spacings measured from WAXD as functions of the spacer length n, wherein the data for $n \leq 4$ correspond to the first order diffraction (i.e., smectic layer spacing) and that for $n \geq 6$ correspond to the second order diffraction (i.e., d_{20} of the rectangular lattice). As mentioned above, P*n*s with $n \leq 4$ form SmAd. Thus a half of the slope (i.e., 0.07 nm/methylene unit) represents the increment caused by adding one methylene unit. This value is smaller than that of 0.125 nm/methylene unit for the spacer with all-trans conformation, implying that the spacers adopt some gauche conformation. For P*n* with $n \geq 6$ formed 2D centered rectangular scaffold of main chain (see Figures 7a and b), the value of d_{20} in fact represents a half of the side-chain length. It increases with *n* with *a* slope of 0.093, also smaller than 0.125, implying the existence of the gauche conformations in the spacer. On the other hand, the short axis *b* of 2D centered rectangular lattice determined based on WAXD results hardly change with n. It means that for $n \geq 6$ P*n*s always have four layers of biphenyl parallel stack in the rectangular lattice.[36]

Table 2. The detail WAXD data for P*n*.

Sample	The value of d_{hk}[a] (nm)	Lattice	Lattice Parameters[b] (nm)
P2	d_{01} = 3.65 d_{02} = 1.82 d_{03} = 1.29	Lamellar	Layer spacing = 3.65
P4	d_{01} = 3.93 d_{02} = 1.96 d_{03} = 1.33	Lamellar	Layer spacing = 3.93
P6[c]	d_{20} = 2.76 d_{11} = 1.96 d_{31} = 1.43 d_{40} =1.38	Rectangular	a = 5.52 b = 2.15
P8	d_{20} = 2.98 d_{11} = 2.05 d_{31} = 1.55 d_{40} = 1.52	Rectangular	a = 5.96 b = 2.18
P10	d_{20} = 3.13 d_{11} = 2.08 d_{31} = 1.62 d_{40} = 1.57	Rectangular	a = 6.26 b = 2.20

[a] Indices are based on the unit cells proposed.
[b] Obtained via Bragg's formula and the orthorhombic equation.
[c] Obtained from the reference [36].

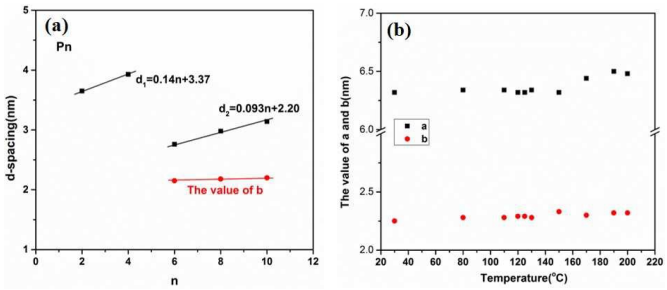

Figure 9. (a) Plot of smectic layer thickness (for n ≤ 4), d20 and calcualted b parameter (for n ≥ 6) vs. the number of methylene units of spacer *n*, (b) Temperature dependence of the calculated *a* and *b* of the rectangular lattice of P10.

It is worth mentioning that the side-chain mesogens of P8 and P10 with longer spacers can SmB-like structure, which is not observed in P6. This outcome suggests that longer spacers promote the ordering of biphenyl groups. We noted that the dimensions of

the rectangular scaffold fabricated by the main-chain changed with the temperature. Figure 9b illustrates the temperature dependence of the calculated value of *a* and *b* of the rectangular lattice for P10. The similar result of P8 is shown in Supporting Information. In Figure 9b, it is observed that slight increases of *a* and *b* occur at 120 °C, correlating to the transition of biphenyl side chain from SmE-like to SmB-like packing; At 150 °C, the significant expansion of a infers the transition of biphenyl side chain from SmB to SmA. The main-chain scaffold of P8 and P10 is always kept until the isotropic transition, which is different from the results of P6. Therefore, P8 and P10 with lengthened spacers can fabricate more stable scaffold of the main chain compared to P6.

Conclusion

In summary, a new series of MCSCLCP with different length of the flexible alkyl spacers, poly(2,5-bis{[n-(4-butoxy-4′-oxybiphenyl)n-alkyl]oxycarbonyl}styrene (P*n*, *n* = 2, 4, 6, 8, 10), have been successfully synthesized via ATRP. The chemical structures of monomers and polymers were confirmed by various characterization techniques. The results indicate that the length of flexible alkyl spacers has great influence on the ordered structure and phase behavior of P*n*. P2 and P4 with the shorter alkyl spacers pack into the SmAd structure. When the flexible spacer becomes longer ($n \geq 6$), the hierarchical ordering with double level and biaxial structure is observed at low temperatures. The phase transition sequence of P8 and P10 from low to high temperature is: the SmE-like structure of side-chain mesogens filled in 2D centered rectangular scaffold of main chain ↔ SmB-like structure of side-chain mesogens filled in 2D centered rectangular scaffold of main chain ↔ isotropic side-chain mesogens filled in 2D centered rectangular scaffold of mainchain ↔ isotropic state. Different from P6 which will have a conventional SmA phase at high temperatures,[36] P8 and P10 can preserve their rectangular main-chain scaffold until the isotropization. On the other hand, the side-chain biphenyl can form hexagonal structure (SmB phase), which is not observed in P6. These differences indicate that longer spacers make the main-chain scaffold more stable and also promote the ordered packing of side-chain mesogens.

Acknowledgements

This research is financially supported by the National Nature Science Foundation of China (21374092 and 21104062), the project of Hunan Provincial Education Department (YB2013B032), Innovation Platform Open Foundation of University of Hunan Province (14K093).

Notes and references

(1) D. J. Simmonds, Liquid Crystal Polymers, From Structures to Applications; Elsevier Applied Science: London and New York, 1992.
(2) C. S. Hsu, Prog. Polym. Sci. 1997, **22**(4), 829-871.
(3) A. Blumstein, Polymeric Liquid Crystals; Plenum Press: New York, 1985.
(4) C. B. Mcardle, Side Chain Liquid Crystal Polymers; Blackie and Son Ltd: Glasgow, U.K., 1989.
(5) V. P. Percec, C. Side Chain Liquid Crystal Polymers; C. B. MacArdle, Ed: Blackie: Glasgow, U.K., 1989.
(6) G. Yang, P.Tang, Y. Yang, Macromolecules 2012, **45**(8), 3590-3603.
(7) H. Yoshida, K. Asakura, J. Fukuda, M. Ozaki, Nat. Commun. 2015, **6**, 1-5.
(8) S. J. Woltman, G. D. Jay, G. P. Crawford, Nat. Mater. 2007, **6**(12), 929-938.
(9) C. Tschierske, Angew. Chem. Int. Ed. 2013, **52**(34), 8828-8878.
(10) N. Koshimizu, Y. Aizawa, K. Sakajiri, K. Shikinaka, K. Shigehara, S. Kang, M. Tokita, Macromolecules 2015, **48**(11), 3653-3661.
(11) M. Ballauff, Angew. Chem. Int. Ed. 1989, **28**(3), 253-267.
(12) K. U. Jeong, B. S. Knapp, J. J. Ge, S. Jin, M. J. Graham, H. Xiong, F. W. Harris, S. Z. D. Cheng, Macromolecules 2005, **38**(20), 8333-8344.
(13) M. Tokita, S. I. Funaoka, J. Watanabe, Macromolecules 2004, **37**(26), 9916-9921.
(14) F. Hessel, H. Finkelmann, Polym. Bull. 1985, **14**(3-4), 375-378.
(15) T. Kato, N. Mizoshita, K. Kishimoto, Angew. Chem. Int. Ed. 2006, **45**(1), 38-68.
(16) Z. Q. Yu, J. W. Y. Lam, K. Zhao, C. Z. Zhu, S. Yang, J. S. Lin, B. S. Li, J. H. Liu, E. Q. Chen, B. Z. Tang, Polym. Chem. 2013, **4**(4), 996-1005.
(17) Z. Q. Yu, J. W. Y. Lam, C. Z. Zhu, E. Q. Chen, B. Z. Tang, Macromolecules 2013, **46**(3), 588-596.
(18) Z. Q. Yu, T. T. Li, Z. Zhang, J. H. Liu, W. Z. Yuan, J. W. Y. Lam, S. Yang, E. Q. Chen, B. Z. Tang, Macromolecules 2015, **48**(9), 2886-2893.
(19) Q. F. Zhou, H. M. Li, X. D. Feng, Macromolecules 1987, **20**(1), 233-234.
(20) C. Ye, H. L. Zhang, Y. Huang, E. Q. Chen, Y. Lu, D. Shen, X. H. Wan, Z. Shen, S. Z. D. Cheng, Q. F. Zhou, Macromolecules 2004, **37**(19), 7188-7196.
(21) S. Pragliola, C. K. Ober, P. T. Mather, H. G. Jeon, Macromol. Chem. Phys. 1999, **200**(10), 2338-2344.
(22) P. Gopalan, L. Andruzzi, X. Li, C. K. Ober, Macromol. Chem. Phys. 2002, **203**(10-11), 1573-1583.
(23) C. Pugh, R. R. Schrock, Macromolecules 1992, **25**(24), 6593-6604.
(24) X. F. Chen, Z. Shen, X. H. Wan, X. H. Fan, E. Q. Chen, Y. Ma, Q. F. Zhou, Chem. Soc. Rev. 2010, **39**(8), 3072-3101.
(25) Q. Zhou, X. Zhu, Z. Wen, Macromolecules 1989, **22**(1), 491-493.
(26) R. Zentel, M. Brehmer, Acta. Polym. 1996, **47**(4), 141-149.
(27) S. W. Cha, J. I. Jin, D. C. Kim, W. C. Zin, Macromolecules 2001, 34(15), 5342-5348.
(28) J. J. Ge, C. Y. Li, G. Xue, I. K. Mann, D. Zhang, S. Y. Wang, F. W. Harris, S. Z. D. Cheng, S. C. Hong, X. Zhuang, Y. R. Shen, J. Am. Chem. Soc. 2001, **123**(24), 5768-5776.
(29) J. J. Ge, A. Zhang, K. W. McCreight, R. M. Ho, S. Y. Wang, X. Jin, F. W. Harris, S. Z. D. Cheng, Macromolecules 1997, **30**(21), 6498-6506.
(30) W. Huang, C. D. Han, Macromolecules 2006, **39**(14), 4735-4745.
(31) X. L. Piao, J. S. Kim, Y. K. Yun, J. I. Jin, S. K. Hong, Macromolecules 1997, **30**(8), 2294-2299.

(32) J. Ruan, J. J. Ge, A. Zhang, J. Shi, S. Y. Wang, F. W. Harris, S. Z. D. Cheng, Macromolecules 2002, **35**(3), 736-745.
(33) M. Zhou, C. D. Han, Macromolecules 2005, **38**(23), 9602-9609.
(34) J. Watanabe, T. Tominaga, Macromolecules 1993, **26**(15), 4032-4036.
(35) H. L. Xie, T. H. Hu, X. F. Zhang, H. L. Zhang, E. Q. Chen, Q. F. Zhou, J. Polym. Sci. Pol. Chem. 2008, **46**(22), 7310-7320.
(36) H. L. Xie, C. K. Jie, Z. Q. Yu, X. B. Liu, H. L. Zhang, Z. H. Shen, E. Q. Chen, Q. F. Zhou, J. Am. Chem. Soc. 2010, **132**(23), 8071-8080.
(37) H. L. Xie, S. J. Wang, G. Q. Zhong, Y. X. Liu, H. L. Zhang, E. Q. Chen, Macromolecules 2011, **44**(19), 7600-7609.
(38) Y. F. Zhu, X. L. Guan, Z. Shen, X. H. Fan, Q. F. Zhou, Macromolecules 2012, **45**(8), 3346-3355.
(39) Y. F. Zhu, W. Liu, M. Y. Zhang, Y. Zhou, Y. D. Zhang, P. P. Hou, Y. Pan, Z. Shen, X. H. Fan, Q. F. Zhou, Macromolecules 2015, **48**(8), 2358-2366.
(40) S. K. Ahn, M. Gopinadhan, P. Deshmukh, R. K. Lakhman, C. O. Osuji, R. M. Kasi, Soft Matter 2012, **8**(11), 3185-3191.
(41) A. A. Craig, C. T. Imrie, Macromolecules 1995, **28**(10), 3617-3624.
(42) M. K. Khan, P. R. Sundararajan, J. Phys. Chem. B. 2013, **117**(18), 5705-5717.
(43) L. Noirez, M. Ungerank, F. Stelzer, Macromolecules 2001, **34**(22), 7885-7893.
(44) K. Okano, Y. Mikami, T. Yamashita, Adv. Funct. Mater. 2009, **19**(23), 3804-3808.
(45) I. Tatsuya, Y. Naitou, M. Tokita, J. Watanabe, Jpn. J. Appl. Phys 2006, **45**, 4991-4993.
(46) J. Watanabe, Y. Nakata, K. Simizu, J. Phys. II France 1994, 4, 581-588.
(47) H. Finkelmann, M. Happ, M. Portugal, H. Ringsdorf, Makromol. Chem. 1978, **179**(10), 2541-2544.
(48) H. Finkelmann, H. Ringsdorf, J. H. Wendorff, Makromol. Chem. 1978, **179**(1), 273-276.
(49) K. Matyjaszewski, J. Xia, Chem. Rev. 2001, **101**(9), 2921-2990.
(50) S. Y. Park, T. Zhang, L. V. Interrante, B. L. Farmer, Macromolecules 2002, **35**(7), 2776-2783.
(51) M. Yamada, A. Hirao, S. Nakahama, T. Iguchi, J. Watanabe, Macromolecules 1995, **28**(1), 50-58.
(52) M. A. Hussein, W. H. D. Jeu, L. Vranichar, S. Pispas, N. Hadjichristidis, T. Itoh, J. Watanabe, Macromolecules 2004, **37**(17), 6401-6407.
(53) D. Kleshchanok, P. Holmqvist, J. M. Meijer, H. N. W. Lekkerkerker, J. Am. Chem. Soc. 2012, **134**(13), 5985-5990.
(54) M. Geppi, A. Marini, C. A. Veracini, S. Urban, J. Czub, W. Kuczyński, R. Dabrowski, J. Phys. Chem. B. 2008, **112**(32), 9663-9676.
(55) C. P. Chai, X. Q. Zhu, P. Wang, M. Q. Ren, X. F. Chen, Y. D. Xu, X. H. Fan, C. Ye, E. Q. Chen, Q. F. Zhou, Macromolecules 2007, **40**(26), 9361-9370.
(56) S. Chen, L. C. Gao, X. D. Zhao, X. F. Chen, X. H. Fan, P. Y. Xie, Q. F. Zhou, Macromolecules 2007, **40**(16), 5718-5725.